

Flexure on Dione: Investigating subsurface structure and thermal history

N.P. Hammond^{a,b,*}, C.B. Phillips^a, F. Nimmo^c, S.A. Kattenhorn^d

^aSETI Institute, 189 Bernardo Avenue, Mountain View, CA 94043, United States

^bBrown University, Providence, RI 02906, United States

^cUniversity of California Santa Cruz, Santa Cruz, CA 95064, United States

^dUniversity of Idaho, Moscow, ID 83844, United States

ARTICLE INFO

Article history:

Received 29 May 2012

Revised 8 December 2012

Accepted 25 December 2012

Available online 8 January 2013

Keywords:

Saturn, Satellites

Geophysics

Thermal histories

Satellites, Surfaces

Tectonics

ABSTRACT

Using stereo generated topography of Dione, a moon of Saturn, we infer flexure across a prominent ridge on the leading hemisphere to estimate local elastic thickness and place constraints on Dione's thermal evolution. Assuming topography is related to the flexing of a broken elastic plate, we estimate an effective elastic thickness of 3.5 ± 1 km. This local estimate is in good agreement with global values derived from long wavelength topography. Corresponding heat fluxes of 25–60 mW/m² are much greater than those expected for a body heated solely from radioactive decay. It would be possible to generate our inferred heat flux values via tidal heating at close to the current orbital eccentricity of Dione, but only if a subsurface ocean were present at the time of flexural deformation.

© 2013 Elsevier Inc. All rights reserved.

1. Introduction

Dione is Saturn's fourth largest moon, with a radius of 561 km and a density of 1480 kg m⁻³ (Thomas, 2010). It is composed mostly of water ice and is possibly differentiated with a silicate core, although its internal structure is highly uncertain (Thomas, 2010). Like many of Saturn's moons, its surface shows evidence of tectonic resurfacing. The trailing hemisphere is covered with numerous extensional fault networks that comprise the region known as wispy terrain (Goff-Pochat and Collins, 2009; Tarlow and Collins, 2010; Wagner et al., 2009). When *Voyager* first imaged these bright linear features, it was suggested they might be geologically young (Smith et al., 1982) and were perhaps cryovolcanic deposits (Plescia, 1983; Stevenson, 1982). *Cassini* imagery later revealed that they have vertical offsets and that many dissect craters, confirming their extensional tectonic origin (Jaumann et al., 2009). Ridges are also present on the leading hemisphere that may have been a result of compression (Collins et al., 2010; Moore, 1984).

Independent of their formation mechanism, topographic features such as ridges and normal faults impose loads on the lithosphere, causing the surface to bend in response (e.g. Watts, 2001). The magnitude and wavelength of this bending is controlled by the effective elastic thickness, the portion of Dione's ice shell that behaves elastically over long timescales (Turcotte and Schu-

bert, 2002). This behavior, known as flexure, has been inferred on Ganymede, Europa, Enceladus and Tethys (e.g. Billings and Kattenhorn, 2005; Giese et al., 2007, 2008; Hurford et al., 2005; Nimmo et al., 2002; Nimmo and Schenk, 2006) and has been used to calculate the elastic thickness and constrain the thermal and orbital evolution of these moons.

In this paper we describe apparent flexure from a tectonic feature on Dione and estimate the local elastic thickness. Our local estimate is consistent with global values of elastic thickness derived from long wavelength topography (Nimmo et al., 2011). We use this estimate to infer the local heat flux, helping constrain the thermal state of the ice shell when this tectonic feature formed. We find that our estimated heat flux can be generated via tidal dissipation at close to the current orbital eccentricity, but only if Dione had a subsurface ocean at the time the estimated heat flux occurred.

2. Background

Imagery from the Cassini Imaging Science Subsystem (ISS) instrument has enabled high resolution mapping of Dione, yet little work has been done to analyze Dione's complex geology utilizing this new resource. Kirchoff and Schenk (2011) classified the surface of Dione into terrain types based on crater density and morphology. Heavily cratered terrain is the oldest and most prominent, with an estimated age of 4 Gyr, using impactor flux case B from Zahnle et al. (2003). Smooth plains and wispy terrain are significantly younger, with less than half the frequency of 10 km diame-

* Corresponding author at: SETI Institute, 189 Bernardo Avenue, Mountain View, CA 94043, United States.

E-mail address: noah_hammond@brown.edu (N.P. Hammond).

ter craters, suggesting approximate ages of 2 Gyr. The absolute ages of these terrains are highly uncertain, since different impactor flux models give a wide range in ages (Dones et al., 2009; Kirchoff and Schenk, 2010; Neukum et al., 2005; Plescia and Boyce, 1985). Regardless, it is clear that at least one tectonic resurfacing event occurred well after Dione's formation (Wagner et al., 2009).

Previous authors have estimated the strain across fault systems in wispy terrain by measuring the width of fault scarps on the camera plane and then correcting for the surface orientation and fault slope in order to calculate the fault throw (Goff-Pochat and Collins, 2009; Tarlow and Collins, 2010). These studies have produced local strain estimates ranging from 0.02 to 0.38. By estimating the duration of rifting, strain measurements can be used to place constraints on the strain rate, which is useful for determining the temperature at the base of the elastic layer (see below). To date, no local elastic thickness estimates have been published for Dione; however, Nimmo et al. (2011) estimated the mean global elastic thicknesses of saturnian satellites by using limb profile data. They associate a break in slope in how roughness varies as a function of wavelength with the transition from flexurally supported to isostatically supported topography, and calculate an elastic thickness of 1.5–5 km for Dione.

We estimate the local elastic thickness from flexure using a method similar to that of Giese et al. (2007), who observed uplift at the flanks of Ithaca Chasma on Tethys and interpreted this as the flexural warping of the lithosphere. Modeling the lithosphere as a broken elastic plate, they estimated the effective elastic thickness T_e to be 5–7 km. They related T_e to the yield strength envelope of the lithosphere, yielding a heat flux of 18–30 mW/m². Chen and Nimmo (2008) subsequently used these results to suggest ancient tidal heating during Tethys' passage through a 3:2 resonance with Dione. Dione and Tethys are moderately tectonically deformed icy satellites of similar size, thus these results provide a useful benchmark for comparison with our results.

3. Observation

Flexural deformation is difficult to measure since its magnitude is often small relative to the topography; therefore, high resolution topographic data are required. We constructed digital elevation models (DEMs) using Ames Stereo Pipeline (Moratto et al., 2010), an automated stereo program that has been tested for accuracy against other elevation data sets for the Moon (Laura et al., 2012). For each stereo pair, camera pointing information is first adjusted with ISIS (Integrated Software for Imagers and Spectrometers) using a control network of up to 10 points. Ames Stereo Pipeline then identifies similar features in both images by using a match correlation window, typically 10 × 10 pixels in size. The parallax between features is used to determine the elevation of each pixel and a sub-pixel refinement process enables increased accuracy. For more detailed descriptions of our stereo technique see Nefian et al. (2009), Segal et al. (2010) and Phillips (2013, in preparation). As input we used overlapping Cassini ISS images with resolutions of 200–300 m/pixel, with a convergence angle of 32°. The vertical accuracy of the resulting DEM is 82 m, based on Eq. (3) from Cook et al. (1996) which accounts for the spacecraft altitudes and differences in viewing angles. For elastic thicknesses of the kind we infer, a load greater than ~1 km in height is required to cause a detectable flexural deflection of the surface.

Our study area is Janiculum Dorsum, a 500 km long, north-south trending ridge on the leading hemisphere's heavily cratered terrain, which may be approximately 4 Gyr old (Fig. 1a). Toward the north the ridge is significantly elevated above the surrounding terrain, reducing in height irregularly toward the south. Janiculum Dorsum is distinct in morphology from ridges observed on Europa

(Collins et al., 2010; Head et al., 1999; Kattenhorn and Hurford, 2009). The ridge has a single peak and is over 30 km wide, compared to ridges on Europa, which range from 200 m to 4 km wide and most commonly appear as a set of parallel ridges (Greeley et al., 2000). However, on both Dione and Europa, parallel depressions can flank ridges. On Europa, previous authors have interpreted these depressions as flexural, which were then used to infer elastic thicknesses (Billings and Kattenhorn, 2005; Hurford et al., 2005).

4. Results

We take four profiles across the northern segment of Janiculum Dorsa where the ridge is at its maximum height. Fig. 1b shows the ridge is 1.5 km high, with a 35 km wide, 300 m deep depression on each side. We assume that this depression results from the flexing of an elastic plate, in which the distance from the load to the inferred forebulge is $\frac{3}{4}\pi\alpha$ for an unbroken plate, where α is the flexural parameter (Turcotte and Schubert, 2002). The flexural parameter is related to the elastic thickness by

$$\alpha = \left(\frac{ET_e^3}{3(1-\nu^2)\Delta\rho g} \right)^{\frac{1}{4}}, \quad (1)$$

where g is gravity, ν is Poisson's ratio, E is Young's Modulus, T_e is elastic thickness and $\Delta\rho$ is the density contrast between the deforming and the overlying material. We use values of $E = 9 \times 10^9$ Pa from laboratory experiments (Gammon et al., 1983), $\Delta\rho = 1000$ kg m⁻³ and $g = 0.233$ m s⁻² (Thomas et al., 2007), and $\nu = 0.3$. The observed distance to the interpreted forebulge implies $\alpha = 15$ km, which in turn yields an elastic thickness of $T_e \approx 1.5$ km. This analytic calculation assumes a line load. For a slightly more accurate estimate, we apply a trapezoidal load shown in green in Fig. 1c and calculate the resulting flexural response using the same approach as Nimmo et al. (2003). Fig. 1c shows that an elastic thickness between 1 and 3 km matches the average profile best, in agreement with the simple analytical calculation. However, if the elastic plate is broken the capacity of the elastic layer to support loads is reduced. The distance from the load to the forebulge in a broken elastic layer is $\frac{1}{2}\pi\alpha$, as opposed to $\frac{3}{4}\pi\alpha$ for an unbroken elastic layer. So to produce the same flexural response, the equivalent thickness of a broken elastic layer must be $(3/2)^{4/3}$ greater (Turcotte and Schubert, 2002). We assume a broken elastic plate and estimate an elastic thickness of 3.5 ± 1 km for Janiculum Dorsum.

5. Discussion

The elastic thickness value of 3.5 ± 1 km for Janiculum Dorsum is the first local elastic thickness estimate for Dione. We ignore membrane stresses caused by the curvature of Dione (Turcotte et al., 1981), which is appropriate given the short wavelength of this feature (Landau and Lifshitz, 1999; Melosh, 2011). The assumption that the lithosphere behaves in a perfectly elastic fashion is a simplification of more complex behavior (Dampitz and Dombard, 2011), but it has been shown to be a good first order approximation of lithospheric structure (Watts, 2001; Melosh, 2011). Our local estimates of elastic thickness are consistent with the global estimate of 1.5–5 km, based on limb profile data (Nimmo et al., 2011). This agreement between two independent methods for estimating elastic thickness serves to strengthen our confidence in these values.

It is desirable to relate effective elastic thickness to heat flux at the time of load emplacement. To do so accurately requires consideration of the time-dependent elasto-visco-plastic relaxation of ice (e.g., Dampitz and Dombard, 2011; Dombard and McKinnon, 2006).

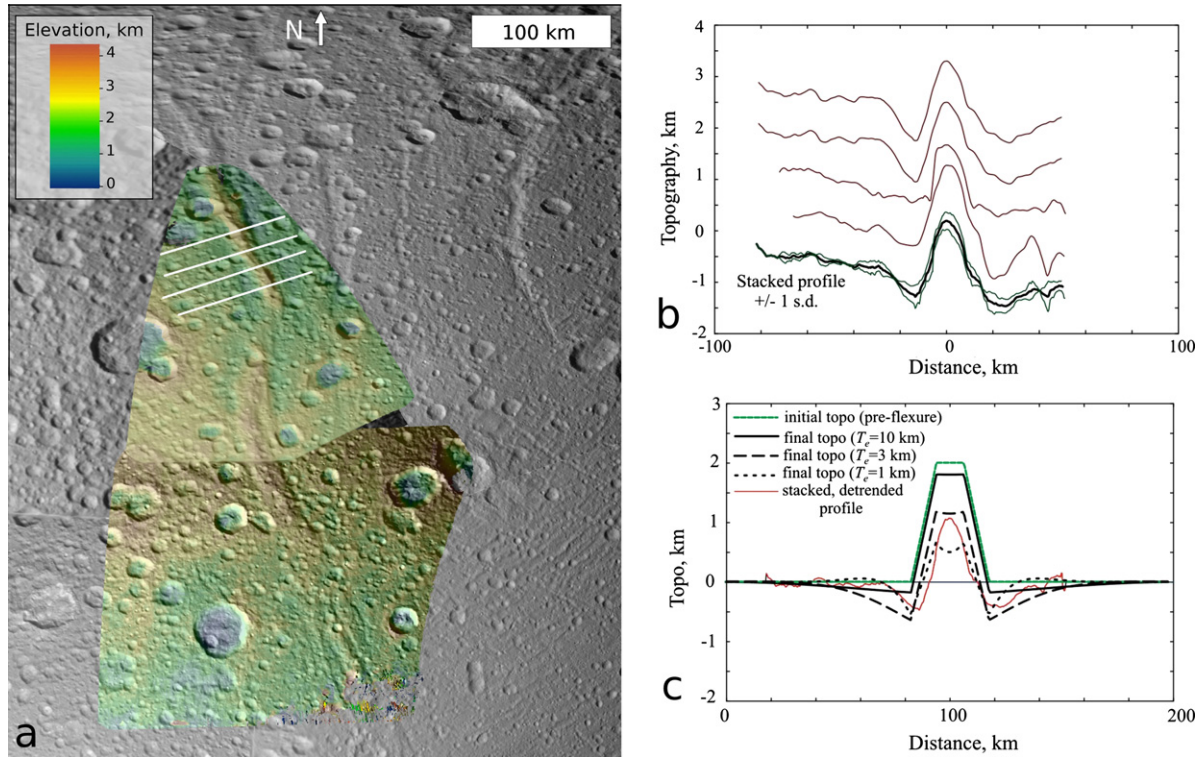


Fig. 1. (a) Digital elevation model of Janiculum Dorsa, located at 150° W 45° N. Constructed with Cassini ISS images N1507741140 and N1665975398, projected over mosaic for regional context. Color denotes elevation; white lines represent profiles. (b) Stacked individual profiles plotted with brown lines. Black and green lines show average profile and ± 1 standard deviation, respectively. (c) Average detrended profile in red compared to modeled trapezoidal load. Green line and solid, dashed and dotted black lines show topography preflexure, and with elastic thicknesses of 10, 3 and 1 km, respectively.

However, simpler approaches, such as the one described below, yield broadly similar results, and facilitate comparative analyses with other works. The heat flux is a function of thermal conductivity, which we assume to vary as $567/T$ (Klinger, 1980), as well as the thermal gradient. To determine the thermal gradient, we assume a surface temperature of 80 K and estimate the temperature at the base of the elastic layer using the approach of Nimmo et al. (2002). Eq. (2) shows how this temperature T_M is dependent on the strain rate $\dot{\epsilon}$, the shear modulus μ , grain size d , the dimensionless Deborah number De , the gas constant R , and rheological properties of the ice, Q , n , A , and p , which vary depending on the dominant deformation mechanism.

$$T_M = \frac{Q}{nR} \left[\ln \left(\frac{3De\mu A^{\frac{1}{n}}}{\dot{\epsilon}^{\frac{1}{n}} d^{\frac{p}{n}}} \right) \right], \quad (2)$$

The shear modulus is computed using our previous values for Young's modulus and Poisson's ratio. We use a Deborah number of 0.01, shown by Mancktelow (1999) to be the transitional value between elastic and viscous behavior. We use rheological constants for dislocation creep, grain boundary sliding, and basal slip from Goldsby and Kohlstedt (2001). Of these rheologies, only grain boundary sliding is grain size dependent. We use a grain size of 1 mm, consistent with grain sizes predicted for evolved ice shells (Barr and McKinnon, 2007).

To estimate strain rate we first estimate the strain at Janiculum Dorsum. Assuming it is a contractional feature, the strain can be expressed as the ratio of the area of the ridge over the area of the underlying elastic layer that experienced shortening. The area of the ridge in the region we infer flexure is ~ 20 km². Using our elastic thickness values of 2.5–4.5 km and assuming the length of the deformation zone is 70 km, which is twice the width of the

ridge, we estimate a compressional strain of 0.06–0.11, similar to previous estimates of extensional strains in wispy terrain of 0.02–0.35 (Goff-Pochat and Collins, 2009; Tarlow and Collins, 2010). Placing an upper-bound of 4 Gyr as the time scale over which this feature formed, we calculate a lower-bound strain for strain rate of $\sim 10^{-18}$ s⁻¹. If the ridge formed much faster, ~ 0.1 Myr, the strain rate could be as high as 10^{-14} s⁻¹. This range is similar to strain rates that have been assumed for other icy satellites (Dombard and McKinnon, 2001; Giese et al., 2007). Higher strain rates will result in higher heat flux values, so in order to be conservative in our estimate of heat flux, we select an upper bound strain rate of 10^{-16} s⁻¹, corresponding to a formation time of 10 Myr.

Using these values, we use Eq. (2) to calculate the temperature at the base of the elastic layer to be 98–120 K. This range includes the three previously discussed rheological deformation mechanisms. Fig. 2 shows the resulting heat flux as a function of strain rate, with various rheologies represented. Red and blue lines show the estimated heat flux given elastic thicknesses of 2.5 km and 4.5 km, respectively. For a grain size of 1 mm, dislocation creep is the dominant deformation mechanism at the base of the elastic layer, since it requires the lowest T_M . Only at low strain rates and probably unrealistically low grain sizes of 10 μ m or less can grain boundary sliding have a slightly lower T_M , and thus become the dominant deformation mechanism (represented by the alternating dashed/dotted lines in Fig. 3). For strain rates between 10^{-16} and 10^{-18} s⁻¹, and $T_e = 2.5$ km and 4.5 km, we calculate a heat flux of 45–60 mW/m² and 25–35 mW/m², respectively. For faster strain rates, or for an intact plate model, the corresponding heat flux could exceed 80 mW/m².

The expected heat flux from radioactive decay at 4 Gyr before present is ~ 4 mW/m² (Hussmann et al., 2010), assuming an ordin-

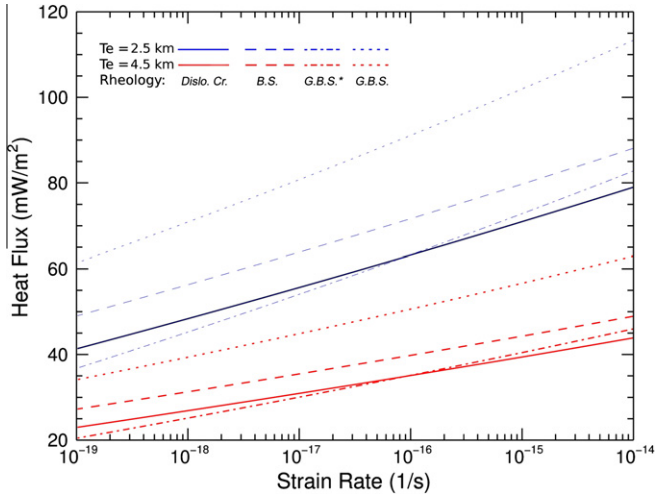


Fig. 2. Blue and red lines show heat flux as a function of strain rate for elastic thicknesses of 2.5 km and 4.5 km, respectively, using Eq. (2) and the method outlined in the text. Solid and dashed lines represent dislocation creep and basal slip-grain boundary sliding, respectively. Dashed/dotted and dotted lines both represent grain boundary sliding-basal slip. They use grain sizes of 10 μm and 1 mm, respectively.

ary chondritic composition for Dione’s silicate material and a rock mass fraction of 0.45 (Thomas, 2010). This is much less than our inferred heat flux values; however, our estimates are similar to those obtained for other moderately deformed icy bodies such as Tethys (Giese et al., 2007). These enhanced heat fluxes may have been caused by a warm upwelling of ice during ridge formation. In fact there are a number of mechanisms proposed for the formation of similar features on other icy satellites which might enhance the local heat flux (Buratti et al., 2012; Head et al., 1999; Kadel et al., 1998; Melosh and Turtle, 2004; Nimmo et al., 2007). Below we explore an alternate possibility, that tidal heating alone could have been sufficient to generate these heat flux values.

The power dissipated in response to tidal forcing, E_t , is given by

$$E_t = \frac{21}{2} \frac{\omega^5 R^5}{G} e^2 \frac{k_2}{Q}, \quad (3)$$

where the relevant terms are: gravitational constant G , the satellite radius R , orbital frequency ω , eccentricity e , the tidal Love number k_2 , and dissipation factor Q (e.g., Murray and Dermott, 1999). To calculate k_2/Q , we used the approach of Roberts and Nimmo (2008) and assume Dione has a silicate core radius of 333 km, a convecting ice shell with a constant viscosity in the range 10^{13} – 10^{14} Pa s, and a near-surface rigid layer 5 km thick. The rigidities of ice and silicate layers are assumed to be 3.5 GPa and 100 GPa, respectively, and the corresponding densities are 950 kg/m^3 and 3500 kg/m^3 .

This structure yields a k_2/Q value of 0.0014–0.013 at the orbital period. If we include a 50 km thick ocean, k_2/Q increases to 0.017–0.12, as a liquid layer decouples the surface from the interior, allowing greater dissipation (Moore and Schubert, 2003). These k_2/Q values are much greater than 3×10^{-4} , the maximum time-averaged k_2/Q value predicted for Dione by Zhang and Nimmo (2009) based on modeling Dione’s orbital evolution following passage through a resonance with Enceladus. This apparent discrepancy can be resolved by noting that k_2/Q tends to increase (Dione becomes more dissipative) if it is being heated; conversely, once heating has ceased after passage through the resonance, k_2/Q will drop rapidly as the interior cools and stiffens. Note that the ocean thickness is not very important; for instance, reducing the thickness from 50 km to 10 km only results in a 25% reduction in the

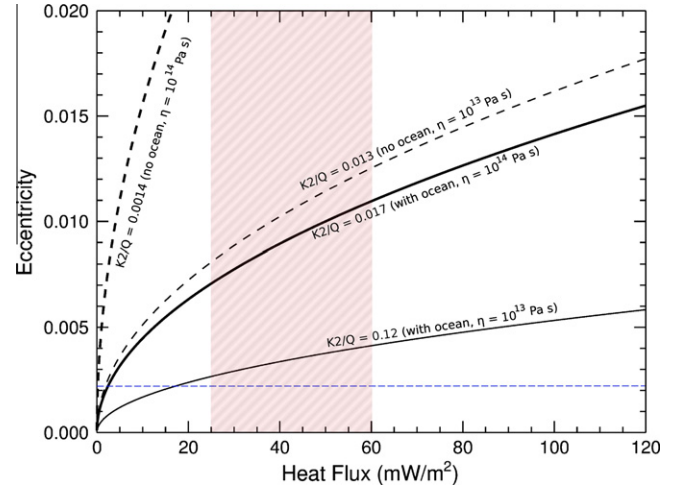


Fig. 3. Plot shows the eccentricity required to generate a given heat flux through tidal heating, for ice shell viscosities of 10^{13} Pa s and 10^{14} Pa s, using Eq. (3). Solid and dashed black lines represent Dione with and without an ocean with k_2/Q values of 0.017–0.12 and 0.0014–0.013, respectively. Dashed blue line indicates Dione’s current eccentricity. The shaded region shows our inferred heat flux range. (For interpretation of the references to color in this figure legend, the reader is referred to the web version of this article.)

value of k_2/Q . In the absence of an ocean, reasonable variations in core parameters will result in changes to k_2/Q of a maximum of a few tens of percent. With an ocean present, variations in core parameters will not affect k_2/Q , because the shell is decoupled from the core.

Fig. 3 shows the eccentricity required to generate a given heat flux on Dione via tidal dissipation, with and without an ocean and for ice shell viscosities of 10^{13} – 10^{14} Pa s. To generate our inferred heat flux via tidal dissipation using a viscosity of 10^{14} Pa s, an ocean would likely be necessary, as the eccentricity required without an ocean is over 10 times the current eccentricity. For a viscosity of 10^{13} Pa s, an eccentricity of about 0.01 is required to generate our inferred heat flux if no ocean is present. However, with an ocean, the required eccentricity drops to 0.003, very close to its current value of 0.0022.

The above results imply that it might have been possible to generate our inferred heat flux values via tidal dissipation without an ocean, but only for the low viscosity case and for eccentricities of ~ 0.01 . It is unclear whether Dione could have experienced eccentricities this large while it was relatively dissipative, although passage through resonances with Enceladus, Mimas and Tethys could have increased its eccentricity appreciably (Zhang and Nimmo, 2009). However, it would be possible to generate our inferred heat flux values for eccentricities much closer to the current value, but only if Dione possessed a subsurface ocean at the time that Janiculum Dorsum formed.

One alternative to tidal dissipation is that the source of heating is local, and does not represent global elevated heat fluxes. However, since our local elastic thickness estimate resembles the global value of Nimmo et al. (2011), it seems likely that our heat flux estimate applies globally. We conclude that our elastic thickness and heat flux estimates are consistent with the presence of a past subsurface ocean on Dione. Elevated heat flux values and a subsurface ocean could also explain highly relaxed craters observed on the surface (Phillips et al., 2012). Furthermore, the refreezing of a 50 km thick ocean on Dione would result in approximately the total surface strain of $\sim 1\%$ measured by Tarlow and Collins (2010) and (Collins, 2010). These observations in combination with our results suggest it is likely Dione had a subsurface ocean at the time Janiculum Dorsum formed.

Acknowledgments

N. Hammond, C. Phillips, and F. Nimmo acknowledge support from the NASA Outer Planets Research Program, Grant #NNX10AQ09G: F. Nimmo was also supported by CDAP #NNX11AK44G.

References

- Barr, A.C., McKinnon, W.B., 2007. Convection in ice I shells and mantles with self-consistent grain size. *J. Geophys. Res.*, 112. <http://dx.doi.org/10.1029/2006JE002781>.
- Billings, S.E., Kattenhorn, S.A., 2005. The great thickness debate: Ice shell thickness models for Europa and comparisons with estimates based on flexure at ridges. *Icarus* 177, 397–412.
- Buratti, B.J., Schenk, P.M., Khurana, K., Moore, J.M., 2012. Dione: The evidence of activity. *Lunar Planet. Sci. XVIII*. Abstract 1659.
- Chen, E.M.A., Nimmo, F., 2008. Implications from Ithaca Chasma for the thermal and orbital history of Tethys. *Geophys. Res. Lett.* 35, L19203. <http://dx.doi.org/10.1029/2008GL035402>.
- Collins, G.C., 2010. Testing Candidate Driving Forces for Faulting on Dione: Implications for Nonsynchronous Rotation and a Freezing Ocean. *AGU (Fall Meet.)*. Abstract P24A-08.
- Collins, G.C. et al., 2010. Tectonics of the outer planet satellites. In: Watters, T.R., Schultz, R.A. (Eds.), *Planetary Tectonics*. Cambridge University Press.
- Cook, A.C., Oberst, J., Roatsch, T., Juamann, T., Acton, C., 1996. Clementine imagery: Selenographic coverage for cartographic and scientific use. *Planet. Space Sci.* 44, 1135–1148.
- Dampitz, A.L., Dombard, A.J., 2011. Time-dependent flexure of the lithospheres on the icy satellites of Jupiter and Saturn. *Icarus* 216, 86–88.
- Dombard, A.J., McKinnon, W.B., 2001. Formation of grooved terrain on Ganymede: Extensional Instability Mediated by Cold, Superplastic Creep. *Icarus* 154, 321–336.
- Dombard, A.J., McKinnon, W.B., 2006. Folding of Europa's icy lithosphere: An analysis of viscous-plastic buckling and subsequent topographic relaxation. *J. Struct. Geol.* 28, 2259–2269.
- Dones, H.C.L., Bierhaus, E.B., Zahnle, K.J., 2009. The Population of Impactors on the Inner Saturnian Satellites. *Am. Astron. Soc. (Fall DPS Meet.)*. Abstract #41, 61.02.
- Gammon, P.H., Kieft, H., Clouter, M.J., Denner, W.W., 1983. Elastic constants of artificial and natural ice samples by Brillouin spectroscopy. *J. Glaciol.* 29, 433–460.
- Giese, B., Wagner, R., Neukum, G., Helfenstein, P., Thomas, P.C., 2007. Tethys: Lithospheric thickness and heat flux from flexurally supported topography at Ithaca Chasma. *Geophys. Res. Lett.* 34, L21203. <http://dx.doi.org/10.1029/2007GL031467>.
- Giese, B., Wagner, R., Hussmann, H., Neukum, G., Perry, J., Helfenstein, P., Thomas, P.C., 2008. Enceladus: An estimate of heat flux and lithospheric thickness from flexurally supported topography. *Geophys. Res. Lett.* 35, L24204. <http://dx.doi.org/10.1029/2008GL036149>.
- Goff-Pochat, N., Collins, B.C., 2009. Strain Measurements across Fault Scarps on Dione. *Lunar Planet. Sci. XL*. Abstract 2111.
- Goldsby, D.L., Kohlstedt, D.L., 2001. Superplastic deformation of ice: Experimental observations. *J. Geophys. Res.* 106, 11017–11030.
- Greeley, R. et al., 2000. Geologic mapping of Europa. *J. Geophys. Res.* 105, 22559–22578.
- Head, J.W., Pappalardo, R.T., Sullivan, R., 1999. Morphological characteristics of ridges and triple bands from Galileo data and assessment of a linear diapirism model. *J. Geophys. Res.* 104, 24223–24236.
- Hurfurd, T.A., Beyer, R.A., Schmidt, B., Preblich, B., Sarid, A.R., Greenberg, R., 2005. Flexure of Europa's lithosphere due to ridge-loading. *Icarus* 177, 380–396.
- Hussmann, H. et al., 2010. Implications of rotation, orbital states, energy sources, and heat transport for internal processes in icy satellites. *Space Sci. Rev.* 153, 317–348.
- Jaumann, R. et al., 2009. Icy satellites: Geological evolution and surface processes. In: Dougherty, M., Esposito, L., Krimigis, S. (Eds.), *Saturn from Cassini-Huygens*. Springer.
- Kadel, S.D., Fagents, S.A., Greeley, R., 1998. Trough-bounding ridge pairs on Europa: Considerations for an endogenic model of formation. *Lunar Planet. Sci. XXIX*. Abstract 1078.
- Kattenhorn, S.A., Hurfurd, T.A., 2009. Tectonics of Europa. In: Pappalardo, R.T., McKinnon, W.B., Khurana, K. (Eds.), *Europa*. University of Arizona Press, pp. 199–236.
- Kirchoff, M., Schenk, P., 2010. Impact cratering records of the mid-sized, icy saturnian satellites. *Icarus* 206, 485–497.
- Kirchoff, M., Schenk, P., 2011. Expanding the global impact cratering record of Saturn's moon Dione: Investigating the geological history. *Euro. Planet. Sci. Conf.*, 2011, p. 1545.
- Klinger, J., 1980. Influence of a phase transition of ice on the heat and mass balance of comets. *Science* 209, 271–272.
- Landau, L.D., Lifshitz, E.M., 1999. *Theory of Elasticity*, second ed. Pergamon, Oxford.
- Laura, J.R., Miller, D., Paul, D.M., 2012. AMES Stereo Pipeline DEM accuracy experiment using LROC-NAC stereopairs and weighted spatial dependence simulation for lunar site selection. *Lunar Planet. Sci. XVIII*. Abstract 2371.
- Mancktelow, N.S., 1999. Finite-element modelling of single-layer folding in elasto-viscous materials: The effect of initial perturbation geometry. *J. Struct. Geol.* 21, 161–177.
- Melosh, H.J., 2011. *Planetary Surface Processes*. Cambridge University Press.
- Melosh, H.J., Turtle, E.P., 2004. Ridges on Europa: Origin by incremental ice-wedging. *Lunar Planet. Sci. XXXV*. Abstract 2029.
- Moore, J.M., 1984. The tectonic and volcanic history of Dione. *Icarus* 59, 205–220.
- Moore, W.B., Schubert, G., 2003. The tidal response of Ganymede and Callisto with and without liquid water oceans. *Icarus* 166, 223–226.
- Moratto, Z.M., Broxton, M.J., Beyer, R.A., Lundy, M.P., Hussmann, K., 2010. Ames Stereo Pipeline, NASA's open source automated stereogrammetry software. *Lunar Planet. Sci. XLI*. Abstract 2364.
- Murray, C.D., Dermott, S.F., 1999. *Solar System Dynamics*. Cambridge University Press.
- Nefian, A.V., Hussmann, K., Broxton, M., To, V., Lundy, M., Hancher, M.D., 2009. A Bayesian formulation for sub-pixel refinement in stereo orbital imagery. In: *ICIP'09 Proceedings of the 16th IEEE International Conference on Image Processing*, pp. 2337–2340.
- Neukum, G., Wagner, R.J., Denk, T., Porco, C.C., and Cassini ISS Team, 2005. The cratering record of the major saturnian satellites in comparison: First results from analysis of the Cassini ISS imaging data. *Lunar Planet. Sci. XXXVI*. Abstract 2034.
- Nimmo, F., Schenk, P., 2006. Normal faulting on Europa: Implications for ice shell properties. *J. Struct. Geol.* 28, 2194–2203.
- Nimmo, F., Pappalardo, R.T., Giese, B., 2002. Elastic thickness and heat flux estimates on Ganymede. *Geophys. Res. Lett.* 29 (7), 1158. <http://dx.doi.org/10.1029/2002GL016660>.
- Nimmo, F., Pappalardo, R.T., 2003. Estimates of Europa's ice shell from elastically-supported topography. *Geophys. Res. Lett.* 30. <http://dx.doi.org/10.1029/2002GL016660>.
- Nimmo, F., Spencer, J.R., Pappalardo, R.T., Mullen, M.E., 2007. Shear heating as the origin of the plumes and heat flux on Enceladus. *Nature* 447, 289–291.
- Nimmo, F., Bills, B.G., Thomas, P.C., 2011. Geophysical implications of the long wavelength topography of the saturnian satellites. *J. Geophys. Res.* 116, E11001. <http://dx.doi.org/10.1029/2011JF003835>.
- Phillips, C.B., Hammond, N.P., Robuchon, G., Nimmo, F., Beyer, R., Roberts, J., 2012. Stereo imaging, crater relaxation and thermal histories of rhea and Dione. *Lunar Planet. Sci. XLIII*. Abstract 2571.
- Plescia, J.B., 1983. The geology of Dione. *Icarus* 56, 255–277.
- Plescia, J.B., Boyce, J.M., 1985. Impact cratering history of the saturnian satellites. *J. Geophys. Res.* 90, 2029–2037.
- Roberts, J.H., Nimmo, F., 2008. Tidal heating and the long-term stability of a subsurface ocean on Enceladus. *Icarus* 194, 675–689.
- Segal, A.V., Nefian, A., Moratto, Z., Styer, M., Broxton, M., 2010. An EM model for subpixel refinement with gamma noise distribution. In: *Spring 2010 IEEE International Conference on Robotics and Automation*. Available at: <<http://www.academia.edu/275972>>.
- Smith, A.B. et al., 1982. A new look at the Saturn system: They Voyager 2 images. *Science* 215, 504–536.
- Stevenson, D.J., 1982. Volcanism and Igneous processes in small icy satellites. *Nature* 298, 142–144.
- Tarlow, S., Collins, G.C., 2010. Fault Scarp Offsets and Fault Population Analysis on Dione. *AGU (Fall Meet.)*. Abstract P31B-1602.
- Thomas, P.C., 2010. Sizes, shapes and derived properties of the saturnian satellites after the Cassini nominal mission. *Icarus* 208, 395–401.
- Thomas, P.C., Burns, J.A., Helfenstein, P., Squyres, S., Veverka, J., Porco, C., Turtle, E.P., McEwen, A., Denk, T., Giese, B., Roatsch, T., Johnson, T.V., Jacobson, R.A., 2007. Shapes of the saturnian icy satellites and their significance. *Icarus* 190, 573–584. <http://dx.doi.org/10.1016/j.icarus.2007.03.012>.
- Turcotte, D.L., Schubert, R.J., 2002. *Geodynamics*. Cambridge University Press, New York.
- Turcotte, D.L., Willemann, R.J., Haxby, W.F., Norberry, J., 1981. Role of membrane stresses in the support of planetary topography. *J. Geophys. Res.* 86, 3951–3959.
- Wagner, R.J., Neukum, G., Stephan, K., Roatsch, T., Wolf, U., Porco, C.C., 2009. Tectonic features on Saturn's satellites Dione and rhea: Morphology and stratigraphy derived from Cassini ISS images. *Lunar Planet. Sci. XL*. Abstract 2142.
- Watts, A.B., 2001. *Isostasy and Flexure of the Lithosphere*. Cambridge University Press.
- Zahnle, K., Schenk, P., Levison, H., Dones, L., 2003. Cratering rates in the outer Solar System. *Icarus* 163, 263–289.
- Zhang, K., Nimmo, F., 2009. Recent orbital evolution and the internal structures of Enceladus and Dione. *Icarus* 204, 597–609.